Fast algorithms for elastic-wave-mode separation and vector decomposition using low-rank approximation for anisotropic media[a]

[a]Published in Geophysics, 79, no. 4, C97-C110, (2014)

Jiubing Cheng, Tongji University, and Sergey Fomel, Bureau of Economic Geology, The University of Texas at Austin

ABSTRACT

Wave mode separation and vector decomposition are significantly more expensive than wavefield extrapolation and are the computational bottleneck for elastic reverse-time migration (ERTM) in heterogeneous anisotropic media. We express elastic wave mode separation and vector decomposition for anisotropic media as space-wavenumber-domain operations in the form of Fourier integral operators, and develop fast algorithms for their implementation using their low-rank approximations. Synthetic data generated from 2D and 3D models demonstrate that these methods are accurate and efficient.

INTRODUCTION

Seismic waves are described by the elastic wave equation with P- and S-waves intrinsically coupled. An elastic migration or inversion program should be able to handle both wave modes. Normally the P and S modes are separated and each is treated independently. Otherwise, the two modes are mixed on all wavefield components and cause crosstalk and image artifacts (Yan and Sava, 2009b). In isotropic media, far-field P- and S-wave modes can be separated by taking the divergence and curl in the extrapolated elastic wavefield. It is well known that a shear wave passing through an anisotropic medium can split into two mutually orthogonal waves (Crampin, 1984). Generally the P-wave and the two S-waves in anisotropic materials are not polarized parallel and perpendicular to the wave vectors and can not be fully separated with divergence and curl operations.

To account for seismic anisotropy, wave mode separation concept and approach have been extendedin the past two decades. Dellinger and Etgen (1990) generalize divergence and curl to anisotropic media by constructing the separators in the wavenumber domain, and independently solving the Christoffel equation in each wave propagation direction. For heterogeneous media, these divergence-like and curl-like separators are rewritten by Yan and Sava (2009b) as nonstationary spatial filters determined by the local polarization vectors. Zhang and McMechan (2010) develop

a wavefield decomposition method to separate elastic wavefields into vector P- and S-wave fields for vertically transverse isotropic (VTI) media. Alternatively, we may implicitly achieve partial mode separation during wavefield extrapolation using the so-called pseudo-pure-mode wave equations, and then obtain completely separated wave modes by correcting the polarization projection deviation of the pseudo-pure-mode wavefields from the isotropic reference (Cheng and Kang, 2012, 2013). Although these studies provide significant insights into wave mode separation in anisotropic media, many challenges remain, especially in the computational implementation if the proposed approaches are directly used in practice. For example, mode separation using nonstationary filtering is computationally expensive, especially in 3D. To improve efficiency, Yan and Sava (2011) present a mixed-domain algorithm that resembles the phase-shift plus interpolation (PSPI) scheme from one-way wave equation migration (Gazdag and Sguazzero, 1984). The compromise between accuracy and cost requires to determine the minimal reference models that best represent the true model space, and the choice of the models is case dependent. On the other hand, Zhang and McMechan (2010)'s wavenumber-domain vector decomposition approach is effective when the model can be separated into distinct geologic units. In addition, spectral methods were proposed to provide solutions which can completely avoid the crosstalk between the qP and qS modes in wavefield modeling and reverse-time migration (RTM) (Etgen and Brandsberg-Dahl, 2009; Liu et al., 2009; Chu et al., 2011; Pestana et al., 2011; Fomel et al., 2013; Song et al., 2013). However, these pure-mode solutions fail to provide accurate amplitudes for qP- and qS-waves. For true-amplitude ERTM in anisotropic media, effective mode separation and decomposition are highly required before applying the imaging condition to the extrapolated elastic wavefields (Zhang and McMechan, 2011).

In this paper, we respectively propose fast algorithms for elastic wave mode separation and vector decomposition in 3D heterogeneous transverse isotropic (TI) media. First, we give a brief review of the underlying principles. Then we present space-wavenumber-domain operations for mode separation and vector decomposition in the form of Fourier integral operators, and discuss how to construct efficient algorithms using low-rank approximation (Engquist and Ying, 2008). At the end, we test efficiency and accuracy of the proposed method using synthetic models of increasing complexity.

ELASTIC WAVE MODE SEPARATION

Using the Helmholtz decomposition theory (Morse and Feshbach, 1953; Aki and Richards, 1980), a vector wavefield $\mathbf{U} = \{U_x, U_y, U_z\}$ can be decomposed into a curl-free P-wavefield and a divergence-free S-wavefield: $\mathbf{U} = \mathbf{U}^P + \mathbf{U}^S$. The P- and S-waves satisfy, respectively,

$$\nabla \times \mathbf{U}^P = 0, \qquad \text{and} \qquad \nabla \cdot \mathbf{U} = \nabla \cdot \mathbf{U}^P, \tag{1}$$

and

$$\nabla \cdot \mathbf{U}^S = 0, \qquad \text{and} \qquad \nabla \times \mathbf{U} = \nabla \times \mathbf{U}^S. \tag{2}$$

These equations imply that the divergence and curl operations pass P- and S-wave modes respectively. In the Fourier-domain, equivalent operations are expressed as follows:

$$\tilde{P}(\mathbf{k}) = i\mathbf{k} \cdot \tilde{\mathbf{U}}(\mathbf{k}), \qquad \text{and} \qquad \widetilde{S}(\mathbf{k}) = i\mathbf{k} \times \tilde{\mathbf{U}}(\mathbf{k}), \tag{3}$$

where $\mathbf{k} = \{k_x, k_y, k_z\}$ represents the wave vector and $\tilde{U}(k_x, k_y, k_z)$ is the 3D wavefield in the wavenumber domain. These operations essentially project the elastic wavefield onto the wave vector or its orthogonal directions, thus separate P- and S-waves successfully. In anisotropic media, however, qP- and qS-waves are not generally polarized parallel and perpendicular to the wave vector. Dellinger and Etgen (1990) extended wave mode separation to anisotropic media with the following divergence-like and curl-like operators in the wavenumber-domain,

$$\widetilde{qP}(\mathbf{k}) = i\mathbf{a}_p(\mathbf{k}) \cdot \tilde{\mathbf{U}}(\mathbf{k}), \qquad \text{and} \qquad \widetilde{qS}(\mathbf{k}) = i\mathbf{a}_p(\mathbf{k}) \times \tilde{\mathbf{U}}(\mathbf{k}), \tag{4}$$

where $\mathbf{a}_p(\mathbf{k})$ stands for the normalized polarization vector of qP wave in the wavenumber domain, calculated from Christoffel equation. Note that the second equation of equation 4 separates only the shear part of the elastic wavefields, which contain the fast and low S-waves, i.e., qS_1- and qS_2 modes. Unlike the well-behaved qP mode, the two qS modes do not consistently polarize as a function of the propagation direction (or wavenumber) and thus cannot be designated as SV and SH waves, except in isotropic and TI media (Winterstein, 1990; Crampin, 1991; Dellinger, 1991; Zhang and McMechan, 2010). In this paper, the approaches to separate and decompose qS-waves are restricted to TI anisotropy.

For TI media, one can separate scalar qSV and SH waves by projecting the elastic wavefield onto their polarization directions using

$$\widetilde{qSV}(\mathbf{k}) = i\mathbf{a}_{sv}(\mathbf{k}) \cdot \tilde{\mathbf{U}}(\mathbf{k}), \qquad \text{and} \qquad \widetilde{SH}(\mathbf{k}) = i\mathbf{a}_{sh}(\mathbf{k}) \cdot \tilde{\mathbf{U}}(\mathbf{k}), \tag{5}$$

where $\mathbf{a}_{sv}(\mathbf{k})$ and $\mathbf{a}_{sh}(\mathbf{k})$ represent normalized polarization vectors of the qSV and SH waves, respectively. For heterogeneous TI media, these operations can be expressed as nonstationary filtering in the space domain (Yan and Sava, 2009b). In fact, the cost may become prohibitive in 3D because it is proportional to the number of grids in the model and the size of each filter (Yan and Sava, 2011).

In general, we can determine polarization vectors by solving the Christoffel equation:

$$(\widetilde{\mathbf{G}} - \rho {V_n}^2 \mathbf{I})\mathbf{a}_n = 0, \tag{6}$$

where $\widetilde{\mathbf{G}}$ represents the Christoffel tensor in the Voigt notation with $\widetilde{G}_{ij} = c_{ijkl} n_j n_l$, c_{ijkl} as the stiffness tensor, and n_j and n_l are the normalized wave vector components in j and l directions, with $i, j, k, l = 1, 2, 3$. The parameter $V_n (n = qP, qS_1, qS_2)$ represents phase velocities of qP-, qS_1- and qS_2-wave modes. The Christoffel equation poses a standard 3×3 eigenvalue problem, the three eigenvalues of which correspond to phase velocities of the three wave modes and the corresponding eigenvector $\mathbf{a}_n$ represents polarization direction of the given mode. When shear singularities appear, the coincidence of the longitudinal and transverse polarizations prevents us from constructing

3D global operators to separate qSV and SH waves on the base of the Christoffel solution, and the polarization discontinuity will cause the two modes to leak energy into each other (Dellinger, 1991; Yan and Sava, 2009a; Zhang and McMechan, 2010; Yan and Sava, 2011). Following Yan and Sava (2009a, 2011), we mitigate the kiss singularity at $k_z = \pm 1$ in 3D TI media by using relative qP-qSV-SH mode polarization orthogonality and scaling the polarizations of the qSV- and SH-waves by $\sin\phi$, with ϕ being the polar angle.

ELASTIC WAVE VECTOR DECOMPOSITION

Wavefield decomposition aims achieving mode separation and vector decomposition simultaneously. On the base of the Helmholtz theory and the theory of anisotropic wave mode separation via the Christoffell equation, Zhang and McMechan (2010) develop a new solution to the problem of decomposing an elastic wavefield into P- and S-waves for isotropic and VTI media. We summarize here only their results used for this study.

For isotropic media, the Helmholtz equations for the P-wave are transformed into the wavenumber-domain as,

$$\mathbf{k} \times \tilde{\mathbf{U}}^P = \mathbf{0}, \qquad \text{and} \qquad \mathbf{k} \cdot \tilde{\mathbf{U}} = \mathbf{k} \cdot \tilde{\mathbf{U}}^P. \tag{7}$$

From these equations, the vector decomposition equation of the separated P-wave is given by:

$$\tilde{\mathbf{U}}^P(\mathbf{k}) = \bar{\mathbf{k}}[\bar{\mathbf{k}} \cdot \tilde{\mathbf{U}(\mathbf{k})}]. \tag{8}$$

where $\bar{\mathbf{k}}$ represents the normalized wave vector.

In a TI medium, equation 8 is extended to separate and decompose qP-wave by substituting $\mathbf{a}_p$ for $\bar{\mathbf{k}}$,

$$\tilde{\mathbf{U}}^{qP}(\mathbf{k}) = \mathbf{a}_p(\mathbf{k})[\mathbf{a}_p(\mathbf{k}) \cdot \tilde{\mathbf{U}}(\mathbf{k})]. \tag{9}$$

Similar equations

$$\tilde{\mathbf{U}}^{qSV}(\mathbf{k}) = \mathbf{a}_{sv}(\mathbf{k})[\mathbf{a}_{sv}(\mathbf{k}) \cdot \tilde{\mathbf{U}}(\mathbf{k})], \tag{10}$$

and

$$\tilde{\mathbf{U}}^{SH}(\mathbf{k}) = \mathbf{a}_{sh}(\mathbf{k})[\mathbf{a}_{sh}(\mathbf{k}) \cdot \tilde{\mathbf{U}}(\mathbf{k})], \tag{11}$$

are proposed to decompose qSV and SH waves using their respective polarization vectors. Note that vector decomposition satisfies the linear superposition relation $\tilde{\mathbf{U}} = \tilde{\mathbf{U}}^{qP} + \tilde{\mathbf{U}}^{SH} + \tilde{\mathbf{U}}^{qSV}$, and the separated wavefields are orthogonal to one another and have the same amplitude, phase, and physical units as the input wavefields.

LOW-RANK APPROXIMATION SOLUTIONS

We observe that both elastic wave mode separation and vector decomposition are based on polarization of wave modes, and any wave mode shares the algorithm structure of separation or decomposition. We will use qP-wave as an example.

We first write the equivalent version of the first equation of equation 4 in the space-domain as

$$qP(\mathbf{x}) = \int e^{i\mathbf{kx}} \left[ia_{px}(\mathbf{k})\tilde{U}_x(\mathbf{k}) + ia_{py}(\mathbf{k})\tilde{U}_y(\mathbf{k}) + ia_{pz}(\mathbf{k})\tilde{U}_z(\mathbf{k}) \right] \mathrm{d}\mathbf{k}. \tag{12}$$

To tackle spatial variations of the polarization in heterogeneous media, we extend the integral operators using

$$\begin{aligned} qP(\mathbf{x}) &= \int e^{i\mathbf{kx}} \left[ia_{px}(\mathbf{x},\mathbf{k}) \right] \tilde{U}_x(\mathbf{k})\, \mathrm{d}\mathbf{k} + \int e^{i\mathbf{kx}} \left[ia_{py}(\mathbf{x},\mathbf{k}) \right] \tilde{U}_y(\mathbf{k})\, \mathrm{d}\mathbf{k} \\ &+ \int e^{i\mathbf{kx}} \left[ia_{pz}(\mathbf{x},\mathbf{k}) \right] \tilde{U}_z(\mathbf{k})\, \mathrm{d}\mathbf{k}, \end{aligned} \tag{13}$$

where $a_{px}(\mathbf{x},\mathbf{k})$, $a_{py}(\mathbf{x},\mathbf{k})$ and $a_{pz}(\mathbf{x},\mathbf{k})$ represent the x-, y- and z-components of the normalized polarization vector of qP waves at location $\mathbf{x}$. Compared with nonstationary filtering (Yan and Sava, 2009b), these pseudospectral-like operations are more accurate but less efficient. The computation complexity of the straight-forward implementation is $O(N_{\mathbf{x}}^2)$, which is prohibitively expensive when the size of model $N_{\mathbf{x}}$ is large.

Similarly, from equation 9, we can derive the space-wavenumber-domain operators for decomposing qP-waves. For example, the x-component of qP-wave satisfies,

$$\begin{aligned} U_x^{qP}(\mathbf{x}) &= \int e^{i\mathbf{kx}} \left[a_{px}(\mathbf{x},\mathbf{k}) a_{px}(\mathbf{x},\mathbf{k}) \right] \tilde{U}_x(\mathbf{k})\, \mathrm{d}\mathbf{k} + \int e^{i\mathbf{kx}} \left[a_{px}(\mathbf{x},\mathbf{k}) a_{py}(\mathbf{x},\mathbf{k}) \right] \tilde{U}_y(\mathbf{k})\, \mathrm{d}\mathbf{k} \\ &+ \int e^{i\mathbf{kx}} \left[a_{px}(\mathbf{x},\mathbf{k}) a_{pz}(\mathbf{x},\mathbf{k}) \right] \tilde{U}_z(\mathbf{k})\, \mathrm{d}\mathbf{k}. \end{aligned} \tag{14}$$

Note that more multiplication operations are needed for vector decomposition.

The discrete implementation of each integral operation in equation 13 or 14 naturally arises as a numerical approximation of a continuous Fourier integral operator (FIO) of the general form. Underlying fast solutions to FIOs is a mathematical insight concerning restriction of the integral kernel to subsets of space and wavenumber domains. Whenever these subsets obey a simple geometric condition, the restricted kernel is approximately low rank (Candes et al., 2007; Ying, 2012). Recently, several two-way wave extrapolation operators have been developed with the help of a low-rank approximation of the space-wavenumber-domain wave-propagator matrix in variable and possibly anisotropic media (Fomel et al., 2010, 2013; Song et al., 2011; Song and Alkhalifah, 2013; Alkhalifah, 2013).

For both mode separation and vector decomposition, phase terms in the FIOs are relatively simple and can be absorbed into inverse Fourier transforms. Therefore our main task is to respectively construct low-rank decomposition for the amplitude terms in the kernel. Previously, Fomel et al. (2013) applied low-rank approximation to the phase-only terms in wave extrapolation operators. Any amplitude term bracketed in equations 13 and 14 can be approximated by the following separated representation:

$$W_j(\mathbf{x},\mathbf{k}) \approx \sum_{m=1}^{M} \sum_{n=1}^{N} B(\mathbf{x},\mathbf{k}_m) A_{mn} C(\mathbf{x}_n,\mathbf{k}), \tag{15}$$

in which $j = x, y, z$, N and M represent the rank of this decomposition, $W_j(\mathbf{x}, \mathbf{k})$ represents the mixed-domain mode separation or vector decomposition operator, $B(\mathbf{x}, \mathbf{k}_m)$ is a mixed-domain matrix with reduced wavenumber dimension, $C(\mathbf{x}_n, \mathbf{k})$ is a mixed-domain matrix with reduced spatial dimension, and A_{mn} is a $M \times N$ matrix. The construction of the separated form 15 follows the method of Engquist and Ying (2009). It can be viewed as a matrix decomposition problem, i.e.,

$$\mathbf{W} \approx \mathbf{BAC}, \tag{16}$$

where $\mathbf{W}$ is the $N_\mathbf{x} \times N_\mathbf{x}$ matrix with entries $W_j(\mathbf{x}, \mathbf{k})$, $\mathbf{B}$ is the submatrix of $\mathbf{W}$ that consists of columns associated with $\{\mathbf{k}_m\}$, $\mathbf{C}$ is the submatrix that consists of rows associated with $\{\mathbf{x}_n\}$, and $\mathbf{A} = \{A_{mn}\}$. Physically, a separable low-rank approximation amounts to selecting a set of N ($N \ll N_x$) representative spatial locations and M ($M \ll N_x$) representative wavenumbers. As explained by Fomel et al. (2013) in detail, we first need to restrict the mixed-domain $\mathbf{W}$ to n randomly selected rows. In practice, n can be scaled as $O(r \log N_x)$ and r represents the numerical rank of $\mathbf{W}$. Then we apply pivoted QR algorithm (Golub and Loan, 1996) to find the corresponding columns for $B(\mathbf{x}, \mathbf{k}_m)$. To find the rows for $C(\mathbf{x}_n, \mathbf{k})$, we apply the pivoted QR algorithm to $\mathbf{W}^*$. The algorithm does not require, at any step, access to the full-matrix $\mathbf{W}$, only to its selected rows and columns.

Representation 15 speeds up the computation of the FIOs in equations 13 and 14 since

$$\begin{aligned} &\int e^{i\mathbf{kx}} W_j(\mathbf{x}, \mathbf{k}) \tilde{U}_j(\mathbf{k}) \, \mathrm{d}\mathbf{k} \approx \\ &\sum_{m=1}^{M} B(\mathbf{x}, \mathbf{k}_m) \left(\sum_{n=1}^{N} a_{mn} \left(\int e^{i\mathbf{kx}} C(\mathbf{x}_n, \mathbf{k}) \tilde{U}_j(\mathbf{k}) \, \mathrm{d}\mathbf{k} \right) \right). \end{aligned} \tag{17}$$

The evaluation of the last formula is effectively equivalent to applying N inverse fast Fourier transforms (FFTs). Accordingly, with low-rank approximation, the computation complexity reduces to $O(NN_\mathbf{x} \log N_\mathbf{x})$. In other word, the costs are mainly controled by the model size N_x and the rank N, which depends on the complexity of the anisotropic velocity model. For isotropic models with arbitrary heterogeneity, the rank automatically reduces to 1 because the polarization directions are material-independent. Similarly to the observation by Fomel et al. (2013), there is a natural tradeoff in the selection of N: larger values lead to a more accurate separated representation but require a longer computational time. In the examples of the next section, the ranks are automatically calculated based on the estimate of the approximation accuracy and generally aiming for the relative single-precision accuracy (namely the maximum allowable error in low-rank decomposition) of 10^{-6}. In multiple-core implementations, the matrix operations in equation 17 are easy to parallelize.

For some applications such as ERTM in TI media, one should construct the separated representations of the operator matrixes in advance, and then implement mode separation or/and decomposition of the extrapolated elastic wavefields before applying the imaging condition. To further save computational cost, appropriate relaxing of

the accuracy requirement for low-rank approximation and applying mode separation only every two or three time steps are both good choices in practice.

EXAMPLES

This section contains four examples. They are for 2D and 3D two-layer models, the SEG/Hess VTI model and the BP 2007 TTI model, respectively. We use 10th-order finite-differnece algorithm for elastic wavefield extrapolation. To accurately compare the used CPU times, algorithm parallelization is not considered for wave mode separation and vector decomposition.

A 2D two-layer TI model

We first test our approach on a two-layer TI model with the size of $N_x = 401 \times 401$.The first layer is a VTI medium with $v_{p0} = 2500m/s$, $v_{s0} = 1200m/s$, $\epsilon = 0.25$, and $\delta = -0.25$, and the second layer is a TTI medium with $v_{p0} = 3600m/s$, $v_{s0} = 1800m/s$, $\epsilon = 0.2$, $\delta = 0.1$, and the tilt angle $\theta = 30^\circ$. A point-source is placed at the center of this model. To aim for the relative accuracy, rank $N = M = 2$ is required for both mode separation and vector decomposition. Thanks to small approximation errors in low-rank decompositions (see Figures 1 and Figure 3), we obtain good mode separation and vector decomposition for the synthesized elastic wavefields (see Figures 2 and 4). It took CPU time of 7.5 seconds to construct the separated forms (as equation 15 expressed) of the mode separation matrixes for qP- and qSV-waves. For one time step, it took CPU time of 0.12, 0.21, and 0.33 seconds to extrapolate, separate and decompose the elastic wavefields, repectively.

A 3D two-layer TI model

We also test the mode separation approach on a 3D two-layer TI model, with $v_{p0} = 2500m/s$, $v_{s0} = 1200m/s$, $\epsilon = 0.25$, $\delta = -0.25$ and $\gamma = 0$ in the first layer, and $v_{p0} = 3600m/s$, $v_{s0} = 1800m/s$, $\epsilon = 0.2$, $\delta = 0.1$ and $\gamma = 0.05$ in the second layer. The size of the model is $N_x = 201 \times 201 \times 201$. A displacement source located at the center of the model and oriented at tilt 45° and azimuth 45°. Figure 5 displays the elastic wavefields and the separated qP-, qSV- and SH-wave fields using the low-rank approximate algorithm. Because the substantial increase of the model size, it is still time consuming to separate the 3D wave modes even if the proposed fast algorithm is used. It took 4008.0, 4130.0 and 91.8 seconds to construct the separated forms of the mode separation matrixes for qP-, qSV- and SH-waves, respectively. For one time step, it took 61.4 seconds to extrapolate the elastic wavefield, and 15.2, 15.8 and 6.8 seconds to separate qP-, qSV- and SH-wave fields with the rank $N = M = 2$.

For comparison, we only change the second layer to a TTI medium with a tilt angle $\theta = 30^\circ$ and azimuth $\phi = 30^\circ$ (other paramters continue to use). Figure 6 displays the

corresponding elastic wavefields and their mode separation results. It took 4087.8, 4280.8 and 206.2 seconds to construct the separated forms of the mode separation matrixes for qP-, qSV- and SH-waves, respectively. For one time step, it took 101.0 seconds to extrapolate the elastic wavefield, and 15.2 and 15.8 seconds to separate qP- and qSV-wave modes with the rank $N = M = 2$. It took 14.1 seconds to separate SH-wave with the rank $N = M = 2$. As we observed, the most time-consuming task here is to construct the separated forms of the mode separation matrixes. More CPU time is required to separate SH-wave in 3D TTI media as well.

SEG Hess VTI model

Then we demonstrate the approach in the 2D Hess VTI model (Figure 7). Vertical S-wave velocity is set to equal half the vertical P-wave velocity everywhere. A point-source is placed at location of (13.264, 4.023) km. Figure 7 shows results of mode separation and vector decomposition, with the rank of about 6 in both cases. It took 133.0 seconds to decompose the operator matrixes for mode separation with rank $N = M = 6$, and 154.1 seconds to decompose the operator matrixes for vector decomposition with rank $N, M \in [6, 7]$. For one time step, it took about 2.2, 4.0, and 7.7 seconds to extrapolate, separate and decompose the elastic wavefields, repectively. However, if nonstaionary spatial filtering is used to separate qP- and qSV-waves at every grid-point, it took about 2340.7 seconds to calculate the filters in advance, and about 444.0 seconds with the truncated operator of size 51×51 at each time step during wavefield extrapolation. This indicates that the mixed domain algorithms using low-rank approximation significantly improve the efficiency for wave mode separation. Of course, larger amount of CPU time has been saved for vector decomposition by using the corresponding low-rank approximate algorithm.

BP 2007 TTI model

This example displays the wave mode separation and vector decomposition results in the BP 2007 TTI model (Figure 9). A point-source is placed near the second salt body at the location of (35.625, 5.0) km. Before wavefield extrapolation, separated representations of the operator matrixes are constructed using the low-rank decomposition approach within the computational zone. It took 217.0 seconds to decompose the operator matrixes for mode separation with rank $N, M \in [15, 17]$, and 345.5 seconds to decompose the operator matrixes for vector decomposition with rank $N, M \in [16, 18]$. For one time step, it took 4.3, 16.0 and 34.8 seconds to extrapolated, separate and decompose the elastic wavefields, repectively. From the separated and decomposed wavefields (Figure 10), we can clearly observe the converted waves from the dipping salt flanks. Due to the low velocities of qSV-wave in some directions at some locations, there are numerical dispersion in the qSV-wave fields. In spite of the dispersion, we obtain well separated qP- and qSV-wave fields, as well as their decomposed x- and z-components.

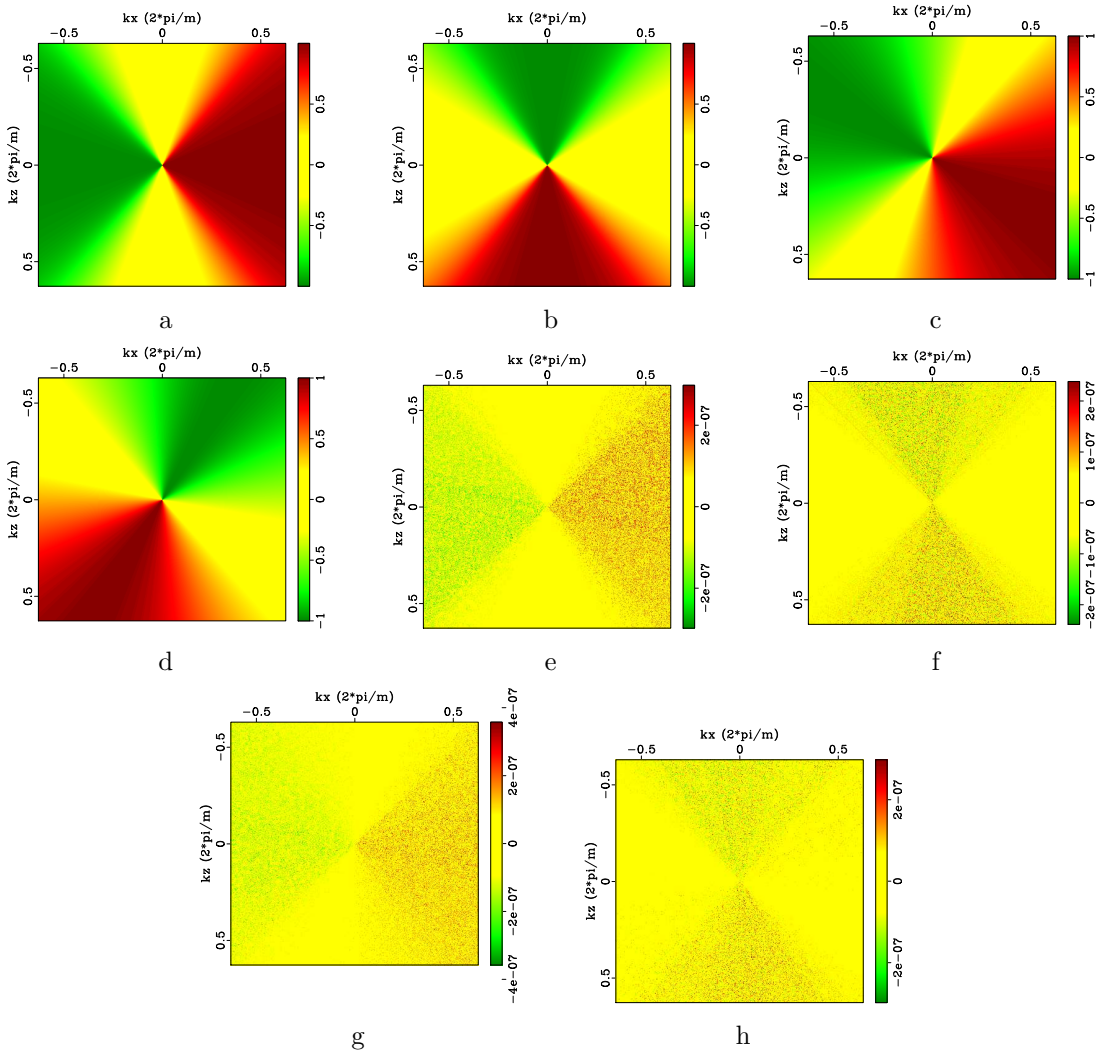

Figure 1: Low-rank approximate mode separators of qP-wave in a 2D two-layer TI model: (a) $a_{px}(\mathbf{x},\mathbf{k})$ and (b) $a_{pz}(\mathbf{x},\mathbf{k})$ constructed by using low-rank decomposition in the VTI layer; (c) $a_{px}(\mathbf{x},\mathbf{k})$ and (d) $a_{pz}(\mathbf{x},\mathbf{k})$ constructed by using low-rank decomposition in the TTI layer; (e), (f), (g) and (h) represent the low-rank approximation errors of these operators. According to the qP-qSV mode polarization orthogonality, we have the following relations: $a_{svx}(\mathbf{x},\mathbf{k}) = -a_{pz}(\mathbf{x},\mathbf{k})$ and $a_{svz}(\mathbf{x},\mathbf{k}) = a_{px}(\mathbf{x},\mathbf{k})$. Therefore, the above pictures also demonstrate the low-rank approximate separators and their errors for qSV-wave.

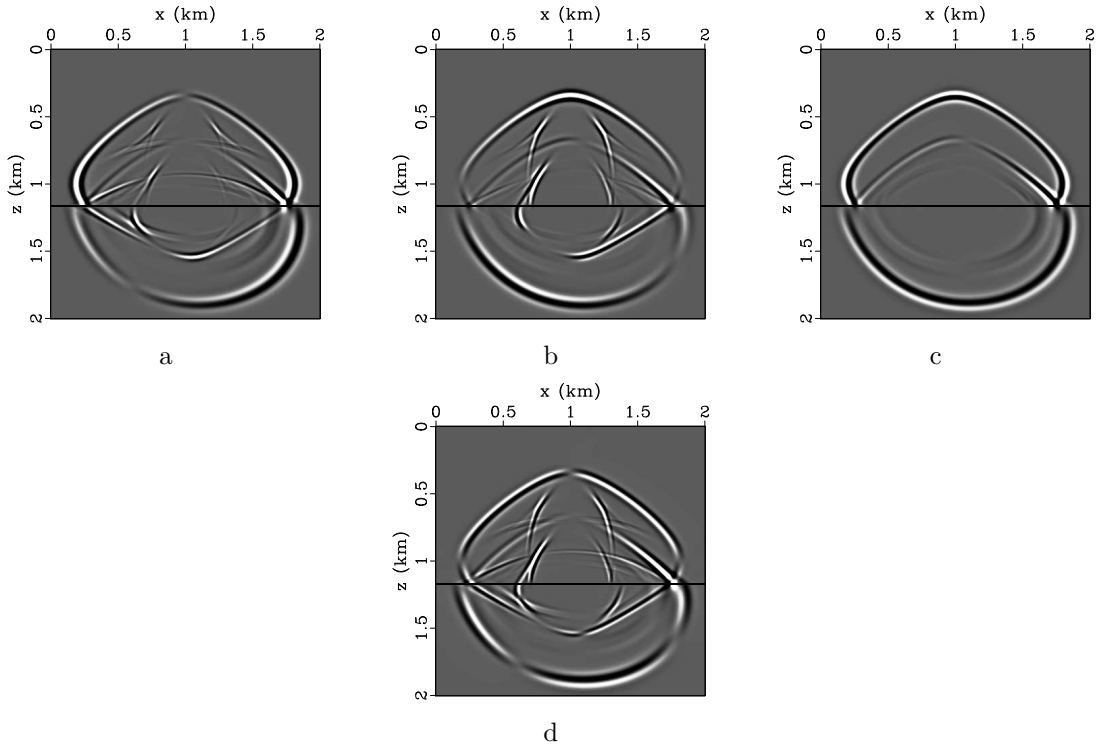

Figure 2: Elastic wave mode separation in the two-layer TI model: (a) x- and (b) z-components of the synthetic elastic displacement wavefields synthesized at 0.3s; (c) and (d) are the separated scalar qP- and qSV-wave fields using low-rank approximation.

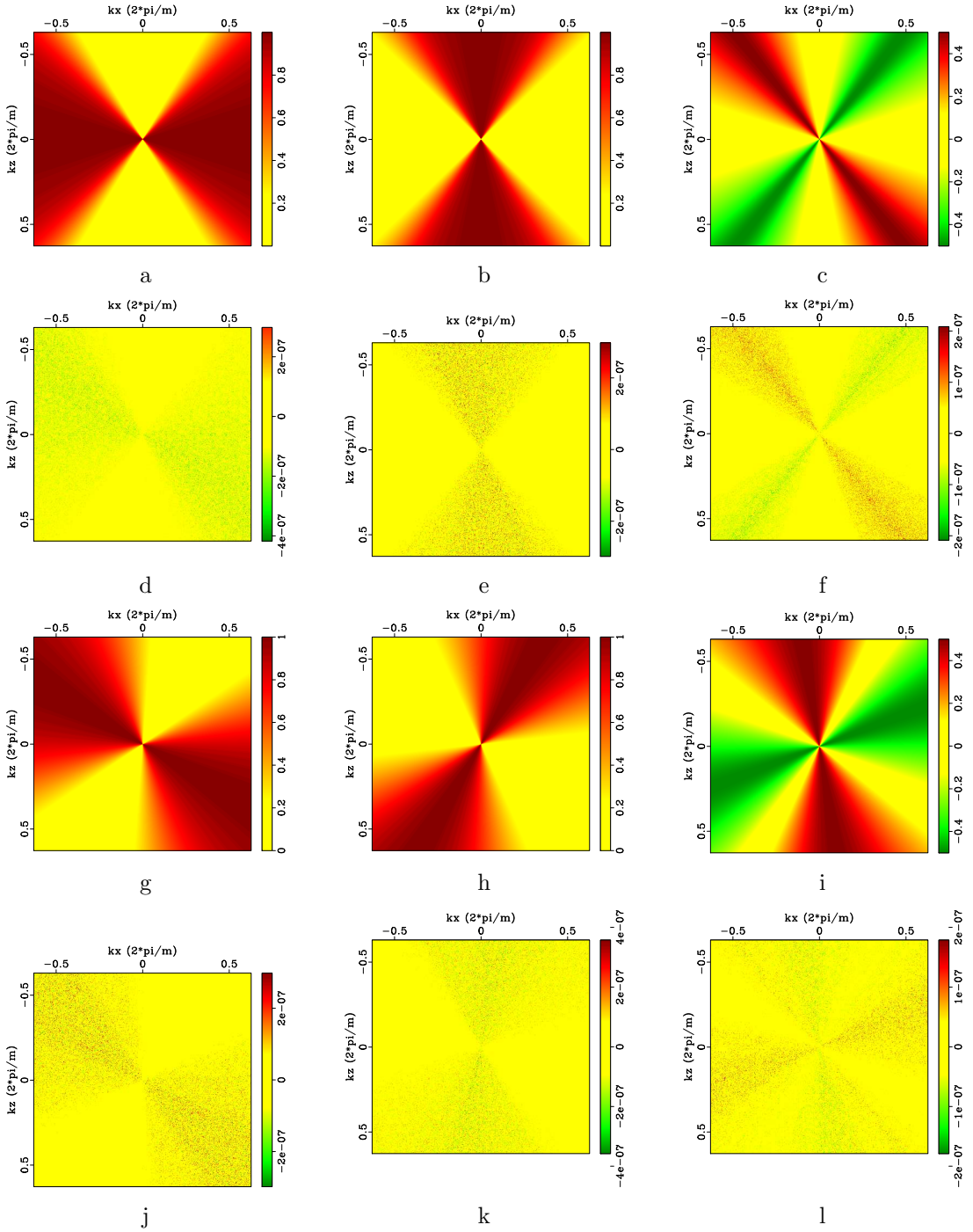

Figure 3: Low-rank approximate vector decomposition operators of qP-wave in the 2D two-layer TI model: (a) $a_{px}(\mathbf{x},\mathbf{k})a_{px}(\mathbf{x},\mathbf{k})$, (b) $a_{pz}(\mathbf{x},\mathbf{k})a_{pz}(\mathbf{x},\mathbf{k})$, and (c) $a_{px}(\mathbf{x},\mathbf{k})a_{pz}(\mathbf{x},\mathbf{k})$, and (e), (f) and (g) represent their low-rank approximation errors in the VTI layer. (h), (i), (j), (k), (l) and (m) are these operators and their low-rank approximation errors in the TTI layer.

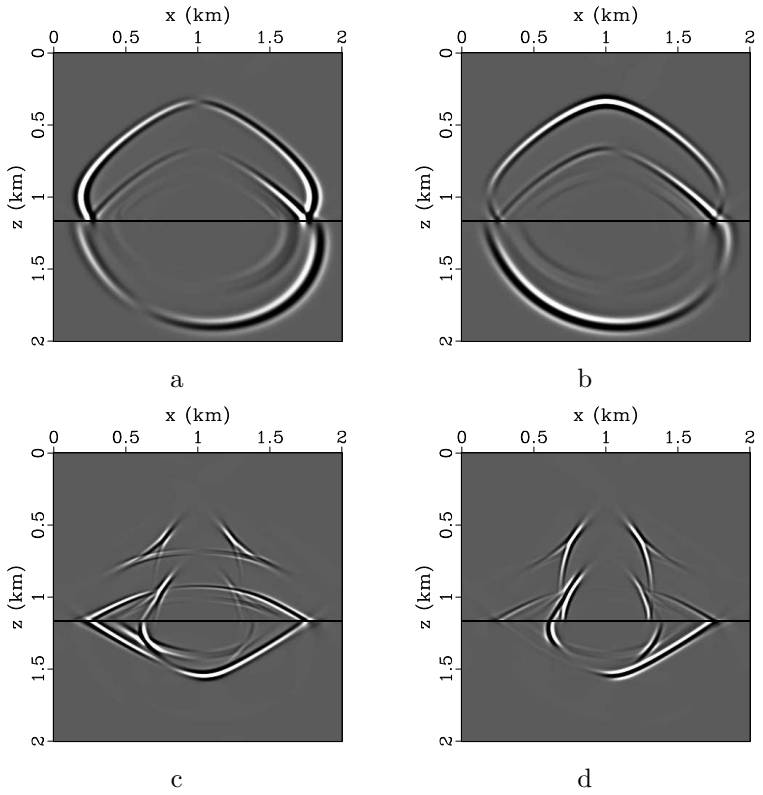

Figure 4: Elastic wave vector decomposition in the two-layer VTI/VTI model: (a) x- and (b) z-components of vector qP-wave fields; (c) x- and (d) z-components of vector qSV-wave fields.

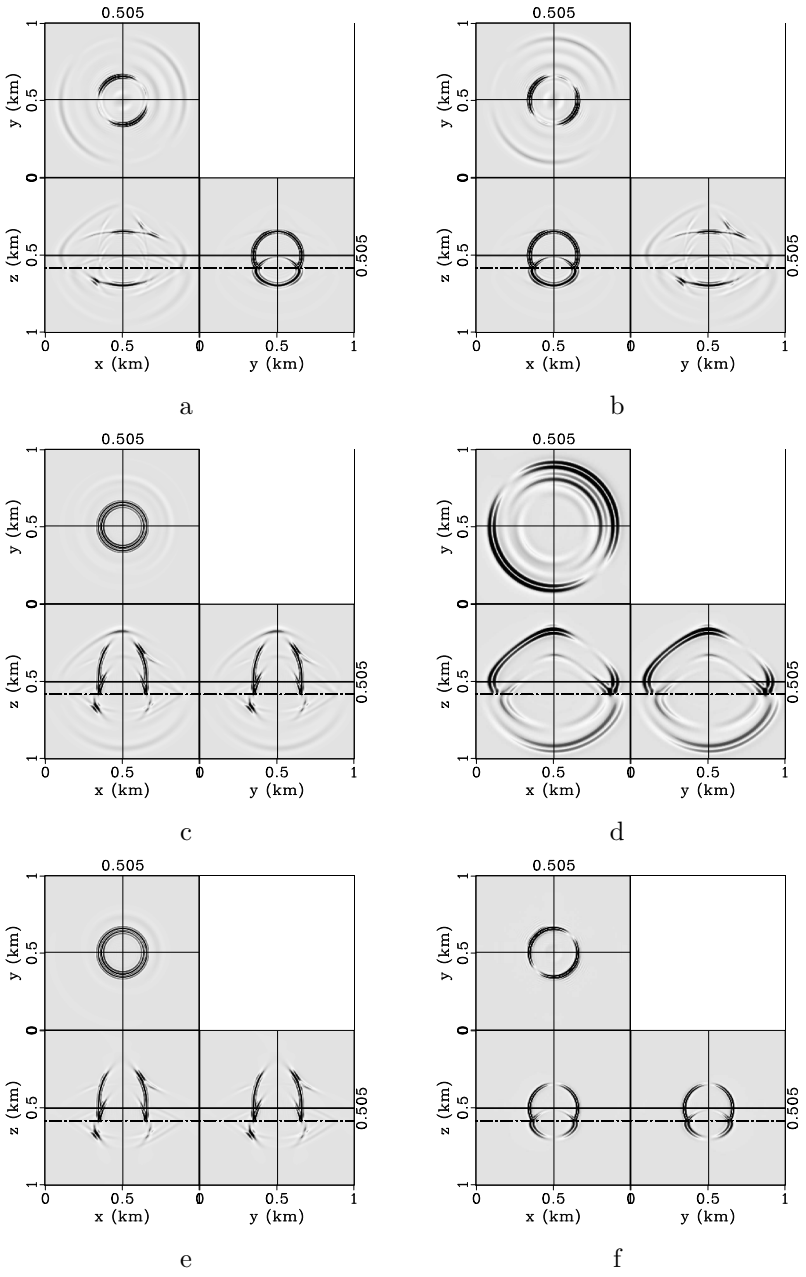

Figure 5: Elastic wave mode separation in the 3D two-layer VTI model: (a) x-, (b) y- and (c) z-components of the synthetic elastic displacement wavefields synthesized at 0.17s; (d) qP-, (e) qSV- and (e) SH-wave fields separated from the elastic wavefields.

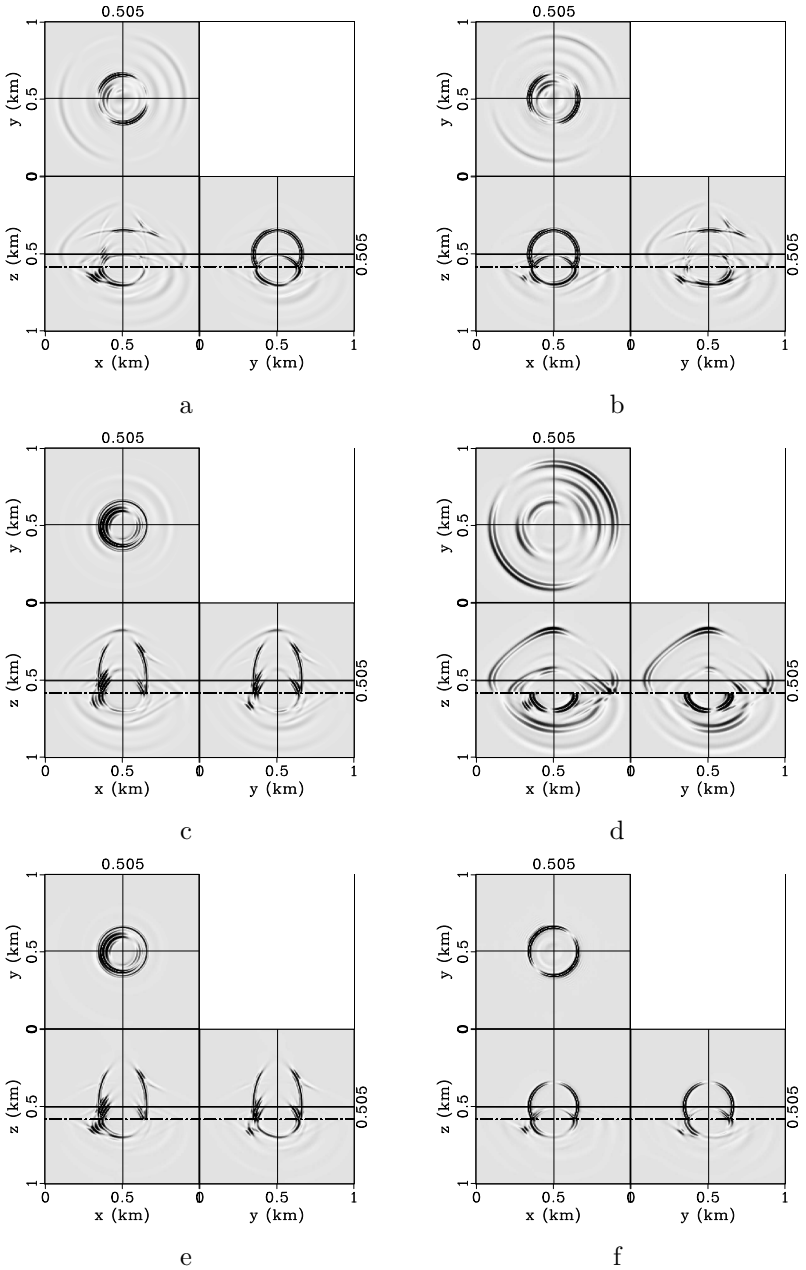

Figure 6: Elastic wave mode separation in the 3D two-layer VTI/TTI model: (a) x-, (b) y- and (c) z-components of the synthetic elastic displacement wavefields synthesized at 0.17s; (d) qP-, (e) qSV- and (e) SH-wave fields separated from the elastic wavefields.

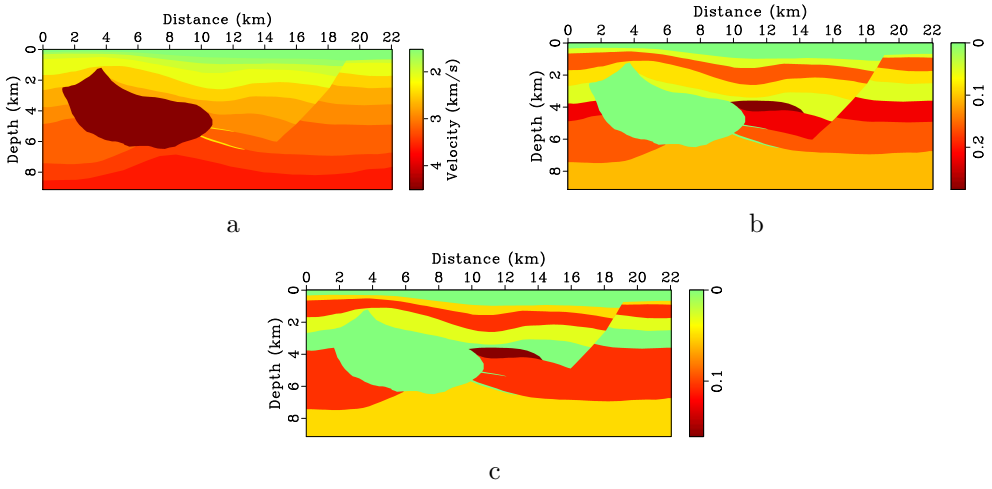

Figure 7: Hess VTI model with parameters of (a) vertical P-wave velocity, Thomsen coefficients (b) ϵ and (c) δ.

Then we investigate the effect of the relative accuracy requirement on wave mode separation. Figure 11 demonstrates the separated P- and qSV-wave fields, and their variations when we relax the approximation level from 10^{-6} to 10^{-3}. It took 174.0 seconds to decompose the operator matrixes for mode separation with rank $N, M \in [7, 8]$, and 345.5 seconds to decompose the operator matrixes for vector decomposition with rank $N, M \in [8, 9]$. And it took 8.0 and 14.9 seconds to separate and decompose the elastic wavefields, repectively. The results are acceptable although more errors are introduced in the separated wavefields when we turn down the relative accuracy requirement.

To further analysize the rough relationship of rank (N, M) with the model complexity, we smooth the BP TTI model by applying a 2D triangle smoothing operator with the radius of 1875m on both x- and z-axes (Figure 12). To maintain the range of the tilt angles, we first double the values of the original model and then apply the smoothing operation for this parameter. Figure 13 demonstrates the synthetic elastic wavefields and the mode separation and vector decomposition results. In this case, it took 207.0 seconds to decompose the operator matrixes for mode separation with rank $N, M \in [13, 14]$, and 310.2 seconds to decompose the operator matrixes for vector decomposition with rank $N, M \in [14, 16]$. It took 15.0 and 29.4 seconds to separate and decompose the elastic wavefields, repectively. We observe that the ranks further decrease to about 12 if we double the smoothing radius to 3750m. For homogeneous TI medium, the ranks automatically decrease to 1. We obtain accurate mode separation and decomposition of the isotropic and elastic wavefields at negligible computational cost with rank $N = M = 1$, if ϵ, δ and θ are all set as 0.0 in the models.

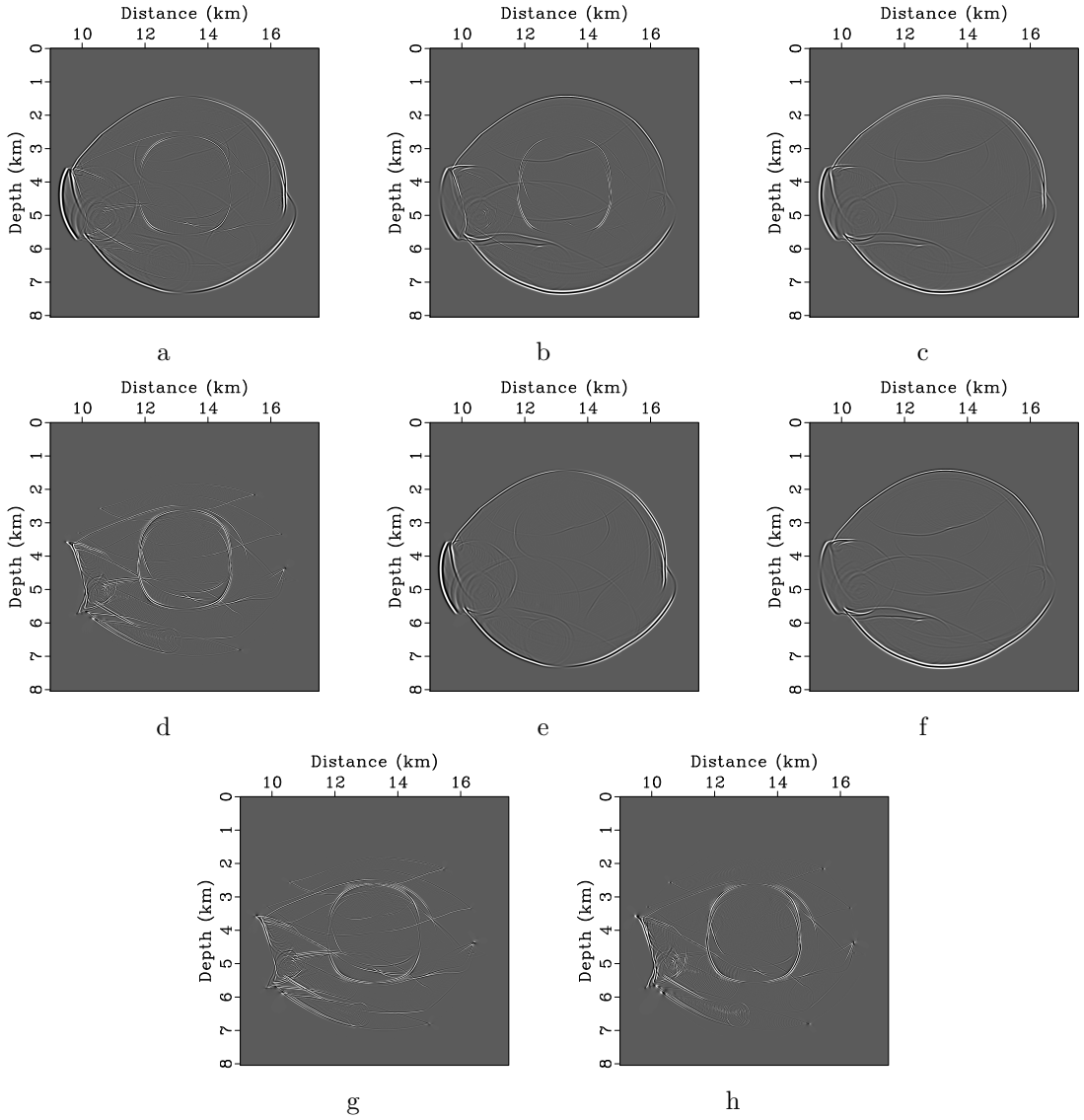

Figure 8: Elastic wave mode separation and vector decomposition in the Hess VTI model: (a) x- and (b) z-components of the synthetic elastic displacement wavefields at 1.1s; (c) and (d) are the separated scalar qP- and qSV-wave fields; (e) x- and (f) z-components of vector qP-wave fields; (g) x- and (h) z-components of vector qSV-wave fields.

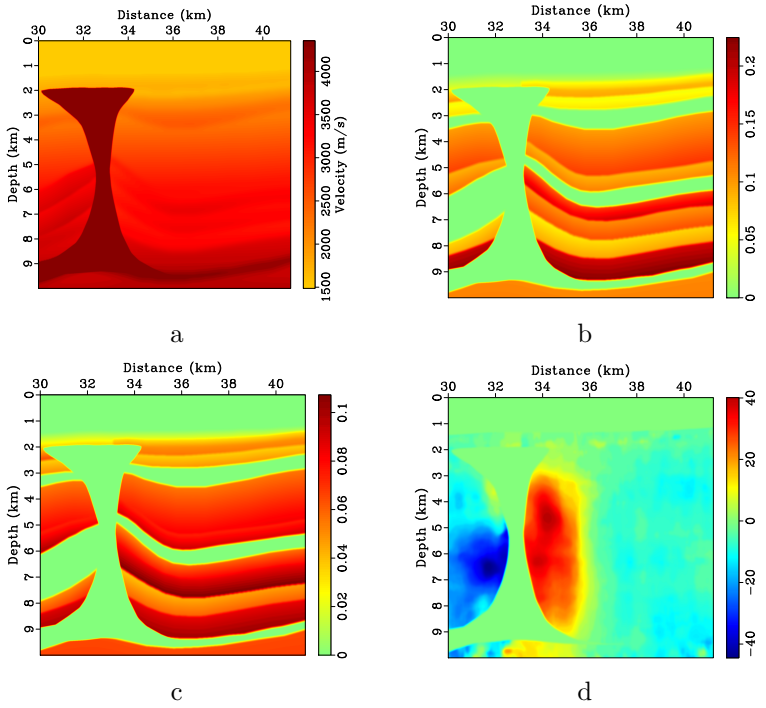

Figure 9: BP 2007 TTI model with parameters of (a) vertical P-wave velocity, Thomsen coefficients (b) ϵ and (c) δ, and (d) tilt angle θ.

CONCLUSIONS AND DISCUSSION

We have developed two fast algorithms for wave mode separation and vector decomposition for heterogeneous TI media. They are based on the low-rank approximation of the space-wavenumber-domain operators, and reduces the cost to that of a small number of FFT operations per time step, corresponding to the approximation rank times the number of components. Synthetic examples show that our approach have high accuracy and efficiency. In general TI media, the rank increases when the models become complex but is always far smallar than the model size. For the 3D elastic wave mode separation and decomposition in heterogeneous TI media, however, constructing the separated representations of the mixed-domain operator matrixes is still time consuming due to the substantial increase of the model size. Parallelizing the algorithm for this procedure may provide a practical solution.

The key concepts of mode separation and vector decomposition are based on polarizations. Unlike the well-behaved P-wave mode, the S-wave modes do not consistently polarize as a function of the propagation direction, and thus can not be designated as SV and SH waves, except in isotropic and TI media. For a 3D TI medium, the effects of kiss singularity are mitigated by using the mutual orthogonality among the qP, qSV and SH modes. This procedure only ensures that the two S-modes are accurately separated in kinematics. It is a challenge to find the right solution of the singularity problem and obtain completely separated two S-modes with correct

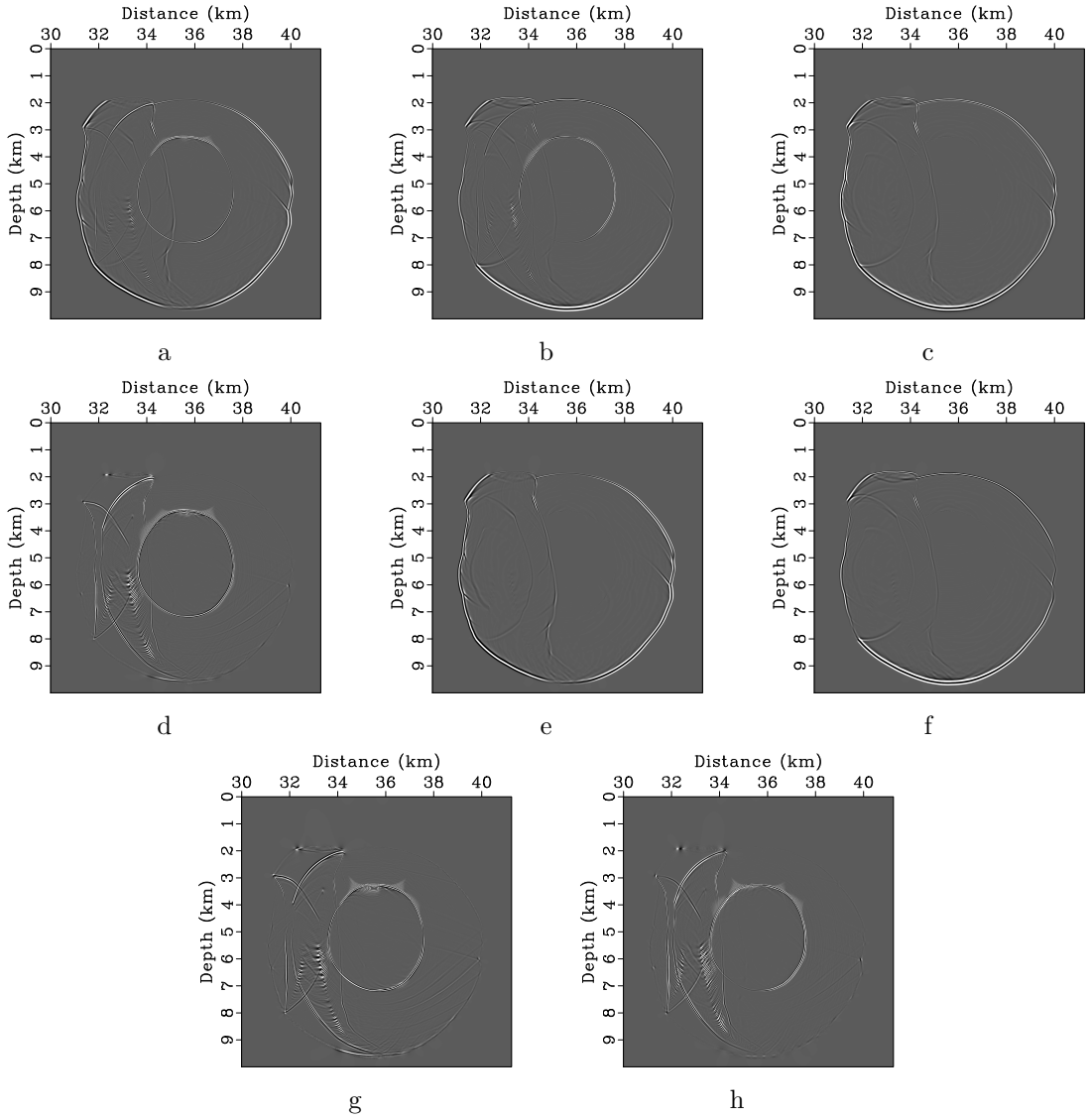

Figure 10: Mode separation and vector decomposition using low-rank approximate algorithms in the BP 2007 TTI model: (a) x- and (b) z-components of the synthetic elastic displacement wavefields at 1.4s; (c) and (d) are the separated scalar qP- and qSV-wave fields; (e) x- and (f) z-components of vector qP-wave fields; (g) x- and (h) z-components of vector qSV-wave fields.

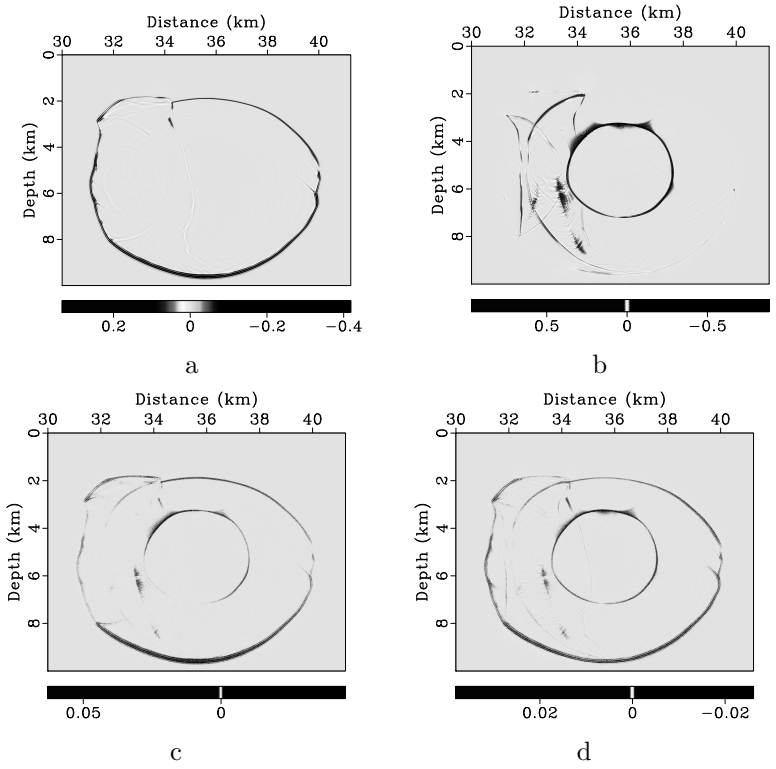

Figure 11: Elastic wave mode separation using low-rank approximation with relaxed accuracy requirements: Separated (a) qP- and (b) qSV-wave fields at the error level of 10^{-3} in low-rank decomposition; Differences of (c) qP- and (d) qSV-wave fields to those separated with the error level of 10^{-6}.

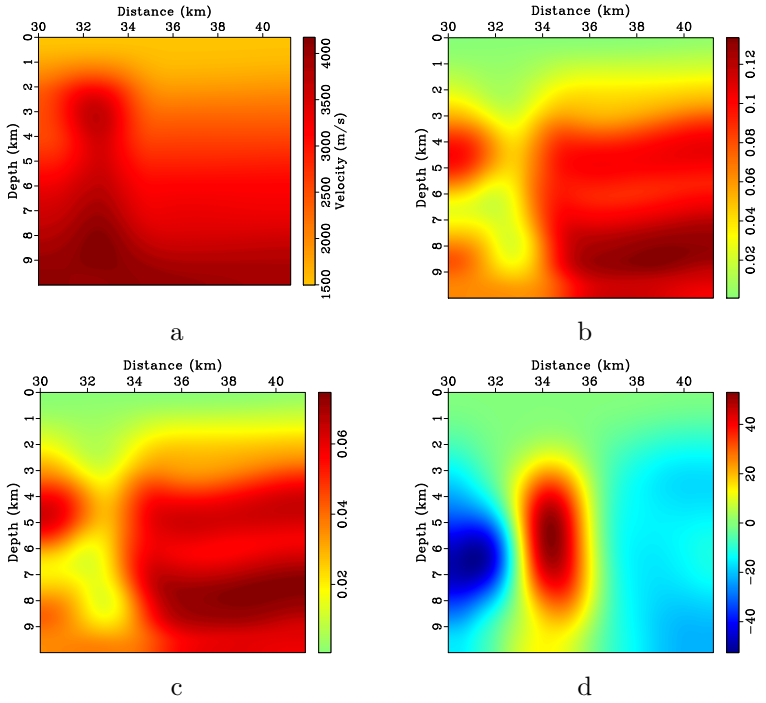

Figure 12: Smoothed BP 2007 TTI model with parameters of (a) vertical P-wave velocity, Thomsen coefficients (b) ϵ and (c) δ, and (d) tilt angle θ. 2D triangle smoothing with the smoothing radius of 1875m on both axis is applied to the paramaters shown in Figure 9.

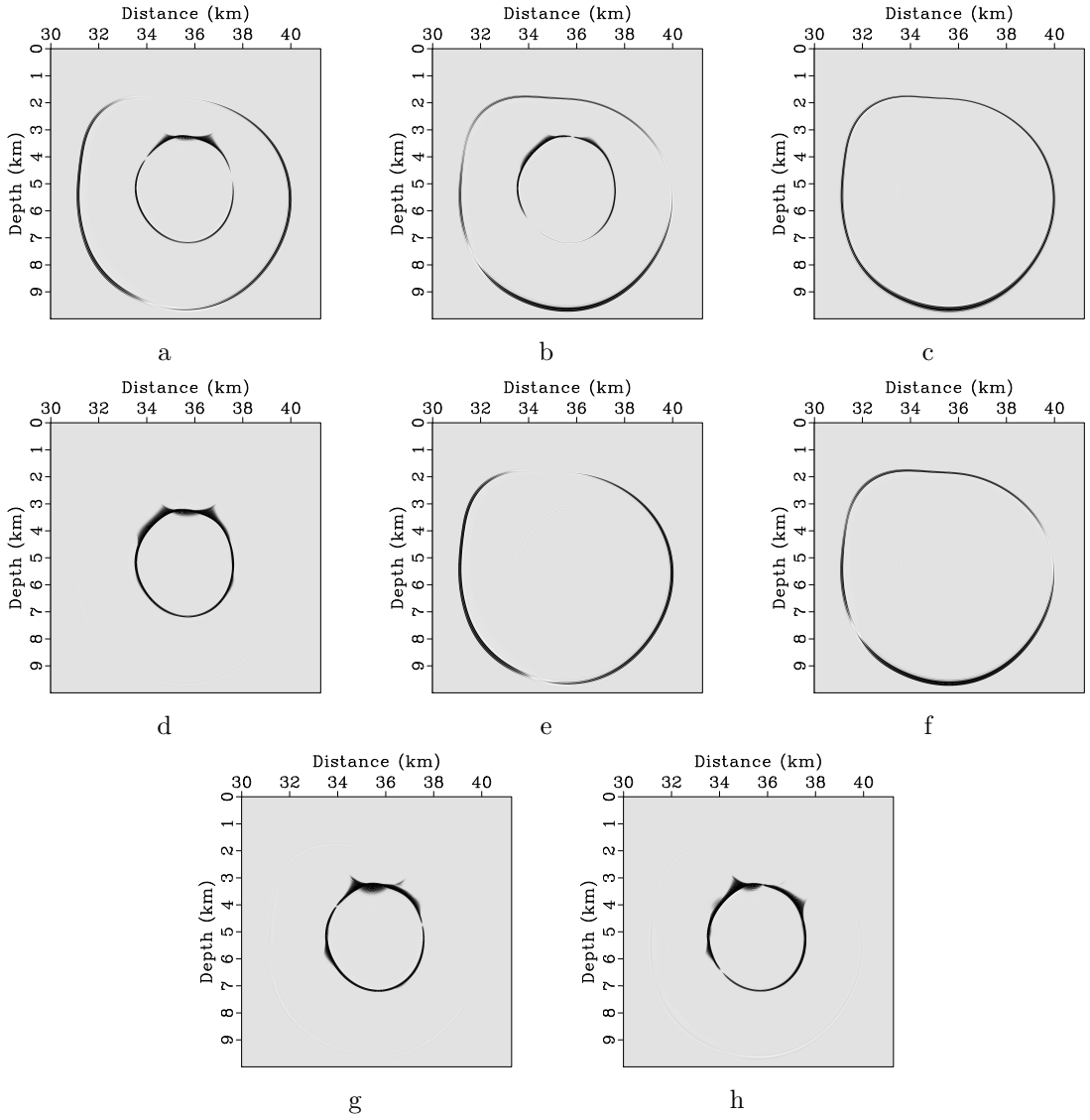

Figure 13: Mode separation and vector decomposition using low-rank approximate algorithms in the BP 2007 TTI model: (a) x- and (b) z-components of the synthetic elastic displacement wavefields at 1.4s; (c) and (d) are the separated scalar qP- and qSV-wave fields; (e) x- and (f) z-components of vector qP-wave fields; (g) x- and (h) z-components of vector qSV-wave fields.

amplitudes.

ACKNOWLEDGMENTS

The first author acknowledges support from the National Natural Science Foundation of China (No.41074083). and would like to thank Xiaolei Song, Jingwei Hu, Siwei Li, Tengfei Wang and Chenlong Wang for useful discussions. Constructive comments by Tariq Alkhalifah, Alexey Stovas, and two anonymous reviewers are much appreciated. We thank SEG, Hess Corporation, and BP for making the 2D VTI and TTI models available.

REFERENCES

Aki, K., and P. Richards, 1980, Quantitative seismology (second edition): University Science Books.

Alkhalifah, T., 2013, Residual extrapolation operators for efficient wavefield construction: Geophysical Journal International, **193**, 1027–1034.

Candes, E., L. Demanet, and L. Ying, 2007, Fast computation of fourier integral operators: SIAM J. Sci. Comput., **29**, 2464–2494.

Cheng, J. B., and W. Kang, 2012, Propagating pure wave modes in general anisotropic media, part I: P-wave propagators: SEG Technical Program Expanded Abstracts, http://dx.doi.org/10.1190/segam2012–0616.1.

———, 2013, Simulating propagation of separated wave modes in general anisotropic media, part I: P-wave propagators: Geophysics, **79**.

Chu, C., B. Macy, and P. Anno, 2011, An accurate and stable wave equation for pure acoustic TTI modleing: SEG Technical Program Expanded Abstracts, 179–184.

Crampin, S., 1984, Effective anisotropic elastic constants for wave propagation through cracked solids: Geophysical Journal of the Royal Astronomical Society, **76**, 135–145.

———, 1991, Effects of point singularities on shear-wave propagation in sedimentary basins: Geophysical Journal Internationl, **107**, 531–543.

Dellinger, J., 1991, Anisotropic seismic wave propagation: PhD thesis, Stanford University.

Dellinger, J., and J. Etgen, 1990, Wavefield separation in two-dimensional anisotropic media: Geophysics, **55**, 914–919.

Engquist, B., and L. Ying, 2008, Fast directional multilevel algorithms for oscillatory kernels: SIAM J. Sci. Comput., **29**, 1710–1737.

———, 2009, A fast directional algorithm for high frequency acoustic scattering in two dimensions: Communications Mathematical Sciences, **7**, 327–345.

Etgen, J., and S. Brandsberg-Dahl, 2009, The pseudo-analytical method: Application of pseudo-Laplacians to acoustic and acoustic anisotropic wave propagation: SEG Technical Program Expanded Abstracts, 2552–2556.

Fomel, S., L. Ying, and X. Song, 2010, Seismic wave extrapolation using a lowrank symbol approximation: SEG Technical Program Expanded Abstracts, 3092–3096.

———, 2013, Seismic wave extrapolation using lowrank symbol approximation: Geophysical Prospecting, **61**, 526–536.

Gazdag, J., and P. Sguazzero, 1984, Migration of seismic data by phase shift plus interpolation: Geophysics, **49**, 124–131.

Golub, G., and C. F. V. Loan, 1996, Matrix computations: John Hopkins.

Liu, F., S. Morton, S. Jiang, L. Ni, and J. Leveille, 2009, Decoupled wave equations for P and SV waves in an acoustic VTI media: SEG Technical Program Expanded Abstracts, 2844–2848.

Morse, P. M., and H. Feshbach, 1953, Methods of theoretical physics: McGraw-Hill Book Company.

Pestana, R., B. Ursin, and P. L. Stoffa, 2011, Separate P- and SV-wave equations for VTI media: SEG Technical Program Expanded Abstracts, 163–167.

Song, X., and T. Alkhalifah, 2013, Modeling of pseudoacoustic P-waves in orthorhombic media with a low-rank approximation: Geophysics, **78**, C33–C40.

Song, X., S. Fomel, and L. Ying, 2013, Lowrank finite-differences and lowrank fourier finite-differences for seismic wave extrapolation in the acoustic approximation: Geophysical Journal International, **193**, 960–969.

Song, X., S. Fomel, L. Ying, and T. Ding, 2011, Lowrank finite-difference for wave extrapolation: SEG Technical Program Expanded Abstracts, 3372–3376.

Winterstein, D., 1990, Velocity anisotropy terminology for geophysicists: Geophysics, **55**, 1070–1088.

Yan, J., and P. Sava, 2009a, 3D elastic wave mode separation for TTI media: SEG Technical Program Expanded Abstracts, 4294–4298.

———, 2009b, Elastic wave-mode separation for VTI media: Geophysics, **74**, WB19–WB32.

———, 2011, Improving the efficiency of elastic wave-mode separation for heterogenous tilted transverse isotropic media: Geophysics, **76**, T65–T78.

Ying, L., 2012, A pedestrain introduction to fast multipole methods: Sci. China Math, **55**.

Zhang, Q., and G. A. McMechan, 2010, 2D and 3D elastic wavefield vector decomposition in the wavenumber domain for VTI media: Geophysics, **75**, D13–D26.

———, 2011, Common-image gathers in the incident phase-angle domain from reverse-time migration in 2D elastic VTI media: Geophysics, **76**, S197–S206.